Supporting Information

Casavant et al. 10.1073/pnas.1302566110

SI Materials and Methods

Numerical Simulations. We used Surface Evolver software to perform numerical simulations on the advancement or stalling of the liquid front in suspended microfluidic configurations. In the case of the rail-shaped channels, geometries were defined by creating two parallel rectangular beams. We filled the space between the beams toward one end of the setup with fluid, and the pressure of the outer face was set to zero to simulate an infinite source of fluid. We determined the conditions for which spontaneous capillary flow (SCF) was impossible (i.e., when the liquid front stalled, when an energetic-equilibrium point could be found). When the software was not able to determine an equilibration point, we considered that SCF was possible (i.e., that the energy profile did not contain a minimum and was constantly decreasing). In the case of U-shaped channels, we added a floor with circular apertures joining the bottom of the two beams in the previously defined geometries. Two unique Surface Evolver software scripts were developed to solve the problems of mesh sizes increasing too fast at the triple line in the corners of the U-groove and numerical errors at the advancing triple line over an aperture (*SI Materials and Methods*, *Numerical Simulation* below).

Mold and Microdevice Fabrication. We fabricated the microchannels in polydimethylsiloxane (PDMS; Sylgard 184; Dow Corning). We created the silicon-SU8 molds for the microchannels by spinning SU-8 50 and 100 (Microchem) on 75- and 150-mm-diameter wafers (WRS) according to the manufacturer's specifications (1). Lithography masks were printed by Image-setter, LLC, and we performed the UV exposure with an OMNICure light source (EXFO). After development, we placed the wafer on a hot plate, mixed PDMS curing agent and base silicone elastomer in a 1:10 ratio, and poured degassed PDMS over the mold. We pressed a cellulose acetate sheet on the uncured PDMS, after which we placed a layer of thin silicone foam, an acrylic rectangle, and a 15-kg weight on top. We cured the PDMS at 85 °C for 3 h and peeled the layer off the wafer. PDMS channels used for solvent extraction experiments were coated with 15 μm of parylene C (PD2010; SCS). Channels were plasma-treated after parylene coating at 50 W for 50 s, with an oxygen flow rate of 5 standard cubic centimeters (sccm) (FEMTO; Diener Electronic).

SCF. PDMS microdevices were designed for two sets of validation experiments. Parallel rail suspended microfluidic channels were designed with constant widths ranging from 500 to 1,000 μm in 100-μm intervals with a height of 700 μm. Channels containing apertures in the floor of the channel were designed with a constant height of 700 μm and width of 800 μm with apertures increasing in size from 200 to 800 μm over the course of the channel. To render the surfaces hydrophilic, the devices were subjected to plasma treatment (FEMTO) at 100 W for 50 s, with an oxygen flow rate of 5 sccm. A red aqueous dye (Allura Red) mixed 1:1 with deionized water was added to the device to characterize the SCF.

Suspended μDot Array. We designed a network of channels leveraging the U-shaped channels containing apertures in the floor, such that the apertures connected with a channel in a layer of PDMS below it. Using a series of U-shaped channels in a top layer of PDMS and a series of channels in a bottom layer of PDMS perpendicular to the top channels, we created an array of these apertures, each accessible from the top by one channel and from the bottom by another channel. We created the μDots in the apertures by flowing and polymerizing a plug of gel in them. In this study, we created two μDot arrays, one with 3 channels on top and 3 channels on the bottom, representing a 9-hole μDot array, and the other containing 4 channels on the top and 10 channels on the bottom, representing a 40-hole μDot array. The top U-shaped channels were 20 mm long and 1 mm wide. The bottom channels were 20 mm long and 1.5 mm wide. The input port for both devices had a diameter of 1.5 mm, the outputs for both were 3 mm, and all channels were 500 μm tall. Two μDot designs were demonstrated. The first design was a circle with a 500-μm diameter and a depth of 250 μm. The second design was an ellipse with a short axis of 500 μm, a long axis of 750 μm, and a depth of 250 μm. To make all surfaces hydrophilic, the devices were plasma-treated channel-up at 100 W for 50 s, with an oxygen flow rate of 5 sccm, and placed on top of each other so that the through-holes connected the two channels. The 40-hole array was designed with similar hole considerations as the 9-hole arrays, with longer U-shaped channels to span the extra channels, and they were 50 mm long and 1 mm wide.

μDot Array for Parametric Multiplexing. To expand on the combinatorial assay using the μDot array described in the main text, we prepared three solutions of 2 μm FITC surface-labeled polystyrene particles (Spherotech) (0.1% wt/vol, 0.01% wt/vol, and 0.001% wt/vol), and then mixed the solutions in a 1:1 ratio with 8.8 mg/mL Matrigel (BD Biosciences). These Matrigel solutions were added to the U-shaped top channel of the μDot array and were able to flow over and into the aperture by means of SCF. We subsequently removed the gel from the channels by aspirating the excess, leaving suspended gels in each of the through-holes. We incubated the devices for 20 min at 37 °C. Three solutions of Texas Red dye and 10 kD of dextran (Invitrogen) were added to the bottom channels at concentrations of 10 μM, 2 μM, and 0.4 μM, and were incubated at 37 °C for 30 min. The bottom channels were then washed with PBS before imaging on an Olympus IX-70 microscope with a 10× fluorescent objective (Fig. S4).

Cell Culture. The prostate cancer (PC3-MM2) cell line was maintained in RPMI 1640 medium supplemented with 10% FBS, 100 U/mL penicillin (Gibco), and 100 μL/mL of streptomycin (Gibco), and was incubated at 37 °C in 5% CO_2. Human T47D breast carcinoma cells (generously donated by M. Gould, University of Wisconsin) were cultured in flasks with low-glucose DMEM medium (1.0 mg/mL; Gibco), supplemented with 10% (vol/vol) FBS, 100 U/mL penicillin, and 100 μL/mL of streptomycin, and were incubated at 37 °C and 5% CO_2. NCI-H295A cells (generously donated by the laboratory of G. D. Hammer (University of Michigan, Ann Arbor, MI) were maintained in phenol red-free DMEM/F-12 medium (Sigma–Aldrich) containing 5% (vol/vol) Nu-Serum I (BD Biosciences), 1% ITS+ Premix (BD Biosciences), 100 U/mL penicillin, and 100 μL/mL streptomycin, and were incubated at 37 °C with 5% CO_2. Culture methods were adapted from Samandari et al. (2). All cells were maintained in standard culture flasks before seeding into microchannels.

Microculture for Solvent Extraction. The microchannel array for solvent extraction was created from two layers of PDMS. The bottom layer, forming a channel used for cell culture, was 300 μm deep, 18 mm long, and 1.5 mm wide. The top channel, a U-shaped channel used for pentanol extraction, was 650 μm deep, 12 mm long, and 0.8 mm wide. The apertures connecting the top

and bottom channels were 150 μm in diameter and 170 μm deep, and they were patterned in an array of 2 × 33. NCI-H295A cells were suspended in cell culture medium with or without 0.5 mM 8-bromoadenosine 3′,5′-cyclic monophosphate (Sigma–Aldrich) at a concentration of 2,600 cells/μL, and 13.0 μL of cell suspension was added to the bottom channel of each microfluidic device. To prevent evaporation, the microfluidic device was placed in a Nunc Omnitray (Thermo Fisher Scientific) containing 250 μL of distilled water (50 × 5-μL drops), which was then placed in a larger tray with an additional 90 mL of distilled water and kept in a humidified incubator.

Steroid Extraction from Microculture on Chip. After 48 h in microculture, steroids were extracted from cell culture medium by adding 9 μL of 1-pentanol (Sigma–Aldrich) to the top channel of the microfluidic device. The device was placed on a rocker (Vari mix platform rocker; Thermo Scientific) during extraction. After 30 min, the pentanol was removed from the channel and an additional 9 μL of pentanol was added to the top channel for 30 min, at which point the pentanol was removed and the channel was washed with 9 μL of pentanol. Combined pentanol extracts were stored at −20 °C before HPLC-MS/MS analysis. This experiment was performed three times with two to four replicates within each experiment.

Extraction of Cortisol Standard Solutions on Chip. Cortisol standard solutions were prepared in media used for the NCI-H295A cell culture with 0.1% methanol at the following concentrations: 50 ng/mL, 250 ng/mL, 1,000 ng/mL, and 5,000 ng/mL. Cortisol solution (13 μL) was added to the bottom channel of the microfluidic device, and the device was placed in a humidified Nunc Omnitray within a humidified incubator as described above for 1 h before extraction. Samples were extracted for a total of 1 h following the protocol outlined above. Samples were extracted for an additional 1 h (2 h total) by adding 9 μL of pentanol to the top channel, waiting 1 h, removing the pentanol, and washing the channel with 9 μL of pentanol. Pentanol extracts were stored at −20 °C before HPLC-MS/MS analysis. This experiment was performed using five microfluidic channels for each cortisol concentration.

HPLC-MS/MS Analysis of Pentanol Microfluidic Channel Extracts for Hormones. Microfluidic channel pentanol extracts in polypropylene autosampler vial inserts (National Scientific) were spiked with 5.0-μL aliquots of a mass-labeled internal standard stock solution containing 1,000 ng/mL d_4-cortisol and d_5-testosterone (C/D/N Isotopes) using a glass syringe (Hamilton). Calibration standards were prepared by aliquoting 1-μL, 2-μL, 5-μL, and 10-μL aliquots of standard stock solution containing 1,000 ng/mL cortisol, cortisone, testosterone, and 11-deoxycortisol (Sigma–Aldrich) to vial inserts that had been spiked with mass-labeled internal standard as described above. The vial inserts were then placed into open 1.5-mL microcentrifuge tubes (FisherBrand), and the solvents were reduced to dryness using a TurboVap Solvent Concentrator (Biotage) operating at 30 °C and 5–10 psi nitrogen gas flow. The vial inserts containing the sample residue were then placed into 2-mL amber glass screw-capped autosampler vials (National Scientific) and reconstituted in 30 μL of 18 MΩ/cm water/methanol (80:20 vol/vol; Honeywell B&JI). The reconstituted extracts were then vortexed vigorously for 30 s and stored refrigerated until analysis.

Hormone analysis was performed by binary gradient reversed phase separation of 10-μL injections of extracts through a Kinetex 2.6-μm, 100-A 150 × 4.6-mm C_{18} column at 40 °C (Phenomenex) using an integrated HPLC system (Prominence UFLC XR; Shimadzu) coupled to a quadrupole-linear ion trap mass spectrometer (QTRAP 5500 MS/MS; AB/SCIEX) operating with atmospheric pressure chemical ionization in positive ionization mode. Pertinent mass spectrometer parameter settings are as follows: source temperature = 500 °C, nebulizer gas = 40 psi, collisionally activated dissociation gas = medium setting, corona discharge needle current = 3.0 V, and entrance potential = 10. Additional details for the HPLC-MS/MS analysis, including the HPLC binary gradient pump program and multiple reaction monitoring MS/MS parameters, are listed in Tables S1 and S2.

Imaging. Phase contrast images were taken after 48 h in culture using an Olympus IX70 microscope equipped with an ORCA-AG CCD camera (Hamamatsu) with a 10× phase objective.

Confocal Microscopy. We prepared a red cell-tracker dye solution (Invitrogen) in PBS, flowed it in the top and bottom channels of the μDot array, and incubated the device for 30 min. After washing with PBS, we fixed, permeabilized, and stained the cells by flowing 4% (vol/vol) paraformaldehyde, 0.1% Triton, and DAPI stain, respectively. We imaged the device on a Digital Eclipse C1 Plus confocal microscope (Nikon) with a slice height of 5 μm and a 5-μs pixel dwell time. We read the image stacks using the ImageJ-based software Fiji (Freeware, NIH) and created final rendered images using the freeware OsiriX (Freeware, www.osirix-viewer.com/).

Multiplexing the Effect of ECM Components, Soluble Factors, and Matrix Metalloproteinase Inhibitors on T47D Cell Growth. A stock collagen solution was prepared by mixing collagen type I (10.59 mg/mL, rat tail; BD Biosciences) with 100 mM Hepes buffer in 2× PBS in a 1:1 dilution ratio, and it was incubated inside a bucket with ice for 10 min. Cells were trypsinized and resuspended in serum-free (SF) DMEM medium. FBS and T47D cells were added to the collagen gels, and SF DMEM was used to adjust the final concentrations to 5×10^5 cells/mL, 4% FBS, and 3.0 mg/mL collagen. For experiments that included fibronectin or laminin, either fibronectin (1 mg/mL, human; BD Biosciences) or laminin (1.88 mg/mL, mouse; BD Biosciences) was mixed with the collagen gels, such that the final collagen concentration was 3.0 mg/mL and the final fibronectin or laminin concentration was 100 μg/mL. Gels containing T47D cells were loaded on the bottom channels of the μDot array. After the loading was done, arrays were placed inside an incubator at 37 °C for 10 min to polymerize the collagen gels.

Human mammary fibroblast (HMF) conditioned medium (CM) was collected from a 2D culture of HMFs that were grown in a flask with high-glucose DMEM medium (4.5 mg/mL; Gibco), supplemented with 10% (vol/vol) calf serum (CS) and 1% penicillin/streptomycin. The collected HMF CM was mixed with 25% (vol/vol) fresh medium (4.5 mg/mL glucose, 10% CS, 1% penicillin/streptomycin). A broad-spectrum matrix metalloproteinase (MMP) inhibitor (5.0 mM GM6001; Millipore) was diluted to 5 μM using SF DMEM, mixed with HMF CM to a get final GM6001 concentration of 500 nM, and then mixed with 25% (vol/vol) fresh medium. As a control, fresh DMEM medium was used to treat T47D cells without the influence of MMP inhibitors or growth factors secreted by HMF cells. All soluble formulations (HMF CM, MMP inhibitor medium, and DMEM) were added through the top channels of the μDot arrays, and changed every other day for 7 d.

Analytical Model of SCF in an Open Microfluidic Geometry. We analyze the case of two simple channel geometries for suspended microflows: the rail-shaped channel (a channel devoid of ceiling and floor) and the U-shaped channel with circular apertures in the floor. However, the analysis performed here can be equally performed on any geometry, and thus will be generalized. It is supposed that the liquid originates from a sufficiently large reservoir, such that the pressure at the inlet port is zero, and we

investigate the conditions for SCF. The model consists of calculating the energy variation with an infinitesimal progression of the liquid in the channel inducing the inflow of a volume dV. The internal pressure P at the liquid front is given by Eq. **S1**, where dE/dV is the variation of free energy per unit volume, γ is the surface, and dA is the variation in areas, with the indices L, S, and G representing liquid, solid, and gas phases, respectively:

$$P = \frac{dE}{dV} = \left(\gamma_{SG}\frac{dA_{SG}}{dV} + \gamma_{SL}\frac{dA_{SL}}{dV} + \gamma_{LG}\frac{dA_{LG}}{dV}\right). \quad \textbf{[S1]}$$

Considering that any increase of the solid–liquid surface A_{SL} is made at the expense of the solid–gas surface A_{SG}, we write $dA_{SG} = -dA_{SL}$, and using Young's law with θ being the contact angle of the fluid on the solid surface, we obtain Eq. **S2**:

$$P = \gamma_{LG}\left(\frac{dA_{LG}}{dV} - \cos(\theta)\frac{dA_{SL}}{dV}\right). \quad \textbf{[S2]}$$

With the reservoir pressure being zero, and given that the condition for flow is $P < 0$, the condition for SCF can be written in Eq. **S3**:

$$\frac{dA_{LG}}{dV} < \cos(\theta)\frac{dA_{SL}}{dV}, \quad \textbf{[S3]}$$

Eq. **S3** can be reduced to Eq. **S4**:

$$\frac{dA_{LG}}{dA_{SL}} < \cos(\theta). \quad \textbf{[S4]}$$

For simplicity purposes, we consider here all liquid interfaces to be straight lines without curvature (Fig. S1). The expressions for the surface area variations in the two cases considered here are written in Eq. **S5**, where dx is the length of advancement of the fluid front, p_f is the perimeter of free (unbounded) surfaces, and p_w is the perimeter of wetted surfaces at the cross-sectional plane of the channel at the fluid front:

$$\begin{aligned} dA_{SL} &= p_w dx, \\ dA_{LG} &= p_f dx. \end{aligned} \quad \textbf{[S5]}$$

On elimination of dx in Eq. **S5** and using Eq. **S5**, a global condition for SCF in a suspended microfluidic channel is written in Eq. **S6**:

$$\frac{p_f}{p_w} < \cos(\theta). \quad \textbf{[S6]}$$

SCF Condition in Different Geometries. The condition for SCF derived in Eq. **S6** has two main assumptions: (*i*) The source pressure of the fluid is negligible, and (*ii*) the interfaces are modeled as straight lines. The cross-sectional shape of the channel modeled is divided into two, possibly discontiguous, sections, with one representing the solid walls and the other representing the unbound air–liquid interface. The model developed does not present any restrictions on the number or shape of these sections, provided they do not make the second assumption invalid. We thus find that the equation describing the condition for SCF flow can be written for suspended and open microfluidic systems but can also predict phenomena, such as the Concus–Finn limit and capillary flow in a tube. Several geometries illustrated in Fig. 2 are detailed here.

We can write more specific SCF conditions for different channel geometries. A simple suspended microfluidic system consists of a channel with a rectangular cross-section of width w and height h, devoid of a ceiling and floor. For this geometry, Eq. **S7** provides a condition on w, h, and θ for the occurrence of SCF:

$$\frac{p_f}{p_w} = \frac{w}{h} < \cos(\theta). \quad \textbf{[S7]}$$

For a channel with a rectangular cross-section, devoid of a ceiling (i.e., a U-shaped cross-section), of width w and height h, Eq. **S8** provides a condition for the occurrence of SCF:

$$\frac{p_f}{p_w} = \frac{w}{2h + w} < \cos(\theta). \quad \textbf{[S8]}$$

For a channel with a rectangular cross-section, devoid of a ceiling (i.e., a U-shaped cross-section), of width w and height h, containing a circular aperture of diameter δ in the floor, Eq. **S9** provides a condition predicting the advancement of the fluid front over the aperture at the largest point of the aperture. One complexity in this case, which will be studied in more detail in the following, is the possibility for the liquid to separate into two Concus–Finn filaments for certain values of θ, and thus not validate the second hypothesis developed earlier:

$$\frac{p_f}{p_w} = \frac{w + \delta}{2h + w - \delta} < \cos(\theta). \quad \textbf{[S9]}$$

In a wedge forming an angle of 90° between a floor and a wall, fluid flow can occur (e.g., a Concus–Finn filament). In this case, the width and height of the fluid filament are equal and the condition for flow in a wedge can be written in Eq. **S10**. Interestingly, Eq. **S10** yields the same condition for the extension of filaments in a wedge as the Concus–Finn limit:

$$\frac{p_f}{p_w} = \frac{\sqrt{(2)}}{2} < \cos(\theta) \text{ (i.e., } \theta < 45°). \quad \textbf{[S10]}$$

In a V-shaped groove with a bottom angle Φ, Concus–Finn fluid filaments can extend. We note w as the half-width of the groove in the top and h as the depth of the groove. The condition for flow in the groove can be written in Eq. **S11**. Interestingly, Eq. **S11** yields the same condition for the extension of filaments in a wedge as the Concus–Finn limit for any angle:

$$\frac{p_f}{p_w} = \frac{w}{\sqrt{(h_2 + w^2)}} < \cos(\theta) \left(\text{i.e., } \theta < \frac{\Phi}{2}\right). \quad \textbf{[S11]}$$

Although capillary flow in closed capillary tubes is not an open microfluidic system, it is interesting to find that Eq. **S6** still holds. We write the trivial condition for flow in a closed tube in Eq. **S12** and show that it matches the well-known 90° limit for observing capillary rise in a tube/channel of small dimensions:

$$\frac{p_f}{p_w} = 0 < \cos(\theta) \text{ (i.e., } \theta < 90°). \quad \textbf{[S12]}$$

Numerical Simulation. From a numerical standpoint, two-phase flows are difficult to model: Finite element methods require a bulky 3D meshing of the computational domain; a remeshing that follows the interface motion; and a complicated time-consuming model for the tracking of interface location, such as the level-set model. On the other hand, surface integral methods only require a 2D meshing of the interfaces but cannot deal with viscous and inertial forces. However, these latter models are well adapted for the prediction of equilibrium states of multiphase components occupying a defined domain. From an initial non-equilibrium topological state, an equilibrium shape is searched. In the present study, we use Surface Evolver numerical software,

which is widely used and documented in the literature, and we make use of its potentialities by noting that if an interface is not at equilibrium, it will evolve to minimize its surface energy. In our case, if the computation does not find an equilibrium state, it means that the SCF continues. More specifically, we created Surface Evolver data files describing the geometries studied (i.e., the parallel rail channel and the U-groove with holes) and set up an initial interface at the inlet (the source codes are available at http://mmb.bme.wisc.edu/links/links.htm?id=links). When SCF occurs, the interface moves at each iteration of the numerical simulation, mimicking the progression of the flow, although not respecting the kinetics of the flow. However, for systems in which the time scale of surface tension equilibration is far less than other characteristic time scales (e.g., velocity, inertia), the progression of the simulation resembles the actual progression of the flow. When the interface stops, an equilibrium point has been determined.

Two types of Surface Evolver data files were set up for this study. The first type corresponds to the geometry of parallel rails (i.e., a rectangular cross-section devoid of a floor and ceiling; Fig. S2*A*) with three options: constant gap distance, increasing gap distance (i.e., diverging rails), and decreasing gap distance (i.e., converging rails). The second type corresponds to a groove with a U-shaped cross-section (Fig. S2*A*) pierced with holes in the bottom plane. In both cases, the pressure is set to zero for simulating an infinite reservoir at the inlet and the initial "artificial" interface is flat and located at the channel inlet. The surface tension is applied on the free surfaces (i.e., the "facets" in Surface Evolver terminology). The capillary force at the wall is taken into account by Green's theorem on the edges comprising the liquid–solid–air contact line; thus, the liquid–solid interface facets do not have to be explicitly represented. It can be shown that the free energy to be minimized is

$$E = \gamma_{LG} A_{LG} - \gamma_{LG} \int_{A_{SL}} cos(\theta) dA, \qquad \textbf{[S13]}$$

where A_{LG} is the free liquid surface area, A_{SL} is the surface in contact with the walls, and θ is the Young contact angle (we use the static contact angle because we are looking for the departure from equilibrium). In Eq. **S13**, the first term on the right-hand side corresponds to the surface tension force exerted on the free surface, and the second term corresponds to the capillary constraints. The surface tension and contact angle are parameters that can be easily changed. As a matter of fact, in the SCF problem, the value of the surface tension does not affect the threshold for SCF but only conditions the dynamics of the flow; hence, the surface tension that is taken into account is that of water γ_{LG} = 72 mN/m.

For the parallel rail geometry and a simple U-shaped groove, with a given contact angle (θ = 35°), a comparison between the numerical and theoretical results is shown in Fig. S2*A*. For small dimensions (i.e., <10 μm), the assumption of planar interfaces produces results close to that of Surface Evolver. A discrepancy starts for large dimensions (i.e., more than several hundred micrometers), where the influence of curved interfaces is larger. Nevertheless, the discrepancy remains acceptable to use Eq. **S6** as a design guideline for open microfluidic systems.

Surface Evolver Command Scripts. To solve the flow of fluid over an aperture in the floor of a U-shaped channel, we developed two unique commands to adapt to the particular geometry considered. First, because the "numerically" fast motion of the triple line in the corners of the U-groove produced increasingly large meshes, we implemented a regularization command for the size of the meshes by finding the average length of the edges along the triple line and then refining the longer edges and deleting the shorter edges. Second, because of errors occurring with the advancing triple line at the contact of a hole, we added a command to fix in place the vertices that hit the edge of the hole. These commands are regularly repeated during the iterations of the numerical energy minimization. We performed the rest of the simulation in a similar manner to the rail-shaped simulation. The source codes developed for performing a simulation of a fluid flowing over an aperture are available at http://mmb.bme.wisc.edu/links/links.htm?id=links.

For the flow over an aperture in a U-shaped groove, with a contact angle of θ = 35°, an initial comparison between the theory and the simulation is shown in Fig. S2*B*. A U-shaped groove, 150 μm wide and 250 μm tall, was designed in Surface Evolver, and apertures of increasing diameter were placed on the floor of the channel. The condition for SCF given by Eq. **S9** was plotted in Fig. S2*B*, and Surface Evolver simulations for different ratios of δ/w were performed. Results show that for this geometry, the theory and the simulations are coherent.

Filling an Aperture in a U-Shaped Channel Above Concus–Finn Limit. We have shown in the preceding section that SCF depends on the geometry and on the contact angle. In this section, we investigate SCF in a U-groove with a hole in the bottom plate. This geometry is slightly more complex, given that two modes of flow can occur: one in which the fluid flows over the aperture and the other in which it flows around it without covering it. Thus, we investigate under which conditions the flow is blocked by the aperture, flows over the aperture, separates into two filaments on each side of the aperture, or flows around the aperture and subsequently fills the aperture. The considered geometry is that shown in Fig. 1*C*.

For SCF to occur over an aperture in the floor of a U-shaped channel, SCF must occur first in the "plain" U-groove, which is determined by Eq. **S8**. However, this condition is not sufficient when the triple line reaches the hole. A more restrictive condition is imposed by the presence of the hole. Two situations can occur: The contact angle of the fluid can be lower than the Concus–Finn limit, in which case the fluid front will split into two filaments, or the contact angle of the fluid can be higher than the Concus–Finn limit, in which case the front moves over the hole in a unified way. These two cases are explored here.

Condition for SCF over an aperture for a fluid with a contact angle over the Concus–Finn limit. Let us assume first that the contact angle is above the Concus–Finn limit (i.e., for a 90° corner, $\theta > 45°$). The condition for SCF given by Eq. **S9** can be written:

$$\frac{\delta}{w} = \frac{\cos(\theta)\left(2\frac{h}{w}+1\right)-1}{\cos(\theta)+1}. \qquad \textbf{[S14]}$$

This shows that the SCF condition depends only on three parameters h/w, δ/w, and θ. We can determine a parameter space identifying all the possible geometries given by h/w and δ/w, and plot the line for a specific θ separating the region that supports filling and the region that does not (Fig. S3*A*).

However, the situation is much more complex when the contact angle is below the Concus–Finn limit. In such a case, two filaments stretch in the two corners. These filaments can eventually merge together downstream from the hole and may fill the hole depending on the ratio h/w and the value of the contact angle.

Condition for SCF over an aperture for a fluid with a contact angle below the Concus–Finn limit. In the case in which the contact angle is below the Concus–Finn limit, the fluid front splits in two filaments around the aperture. At this point, the fluid acts as two separate flows in a wedge and does not validate the straight interface assumption used to develop the equation for SCF (Eq. **S6**). Downstream of the aperture, the filaments can continue as filaments without merging, and therefore without filling the U-shaped

channel, or the filaments can grow and merge. For SCF to occur, the fluid must cover the aperture; thus, two conditions need to be validated. The first is the merging of the two filaments downstream of the aperture. The second is the covering of the aperture after the filaments have merged.

If a merging event occurs, and the conditions for SCF are validated (given by Eq. **S6**), the merging will propagate upstream and downstream until the aperture is surrounded by fluid. However, if filaments do not merge, suspended flow downstream of the aperture is disrupted and filling of additional apertures is impossible. Modeling Concus–Finn filaments in the U-shaped channel is a nontrivial problem that depends on static properties of the fluid and the channel (e.g., geometry, surface energy), as well as on dynamic effects due to fluid flow. If we neglect dynamic effects (which is a reasonable assumption in a real channel because the length is not infinite and the flow must stop at one point), the interface will grow until it reaches the top edge of the U-shaped channel. Furthermore, because the pressure at all points of the filament must be null, and therefore the interface is flat, we can calculate the contact point in the floor of the U-shaped channel based on the contact angle of the fluid. If the filament fills more than half of the width of the U-shaped channel, merging with the opposing filament will occur and fluid will fill around the aperture. The condition for filament merging can therefore be written in Eq. **S15**:

$$\frac{h}{w} > \frac{1}{2} tan\theta. \qquad \textbf{[S15]}$$

To identify the conditions for filling of the aperture, we performed numerical simulations using Surface Evolver. Using the same parameter space as in Fig. S6, we explored the conditions for filament merging and aperture filling. We find that SCF can occur for contact angles lower than the Concus–Finn limit for a larger set of geometries (Fig. S3*B*). The combination of the plots in Fig. S3 *A* and *B* allows plotting of the general overview of SCF over an aperture pictured in Fig. 1*C*.

Summary Table Describing Conditions for SCF. The analytical model provided by Eq. **S6**, and applied to specific geometries in Eqs. **S7–S11**, proves to be a general model describing the conditions for SCF in any open suspended microfluidic setup or closed channel in which the capillary action is used to flow a fluid while using a geometry to pin it. The specific conditions for different key geometries have been detailed in Fig. S4, with their corresponding Surface Evolver simulations.

Because SCF over an aperture in the floor of a U-shaped channel contains specific complexities, we summarize the filling dynamics and verify our analytical model with different scenarios for channel and aperture aspect ratios (Fig. S5). A range of geometrical and contact angle conditions was chosen to span most of the useful parameter space. Three channel heights allowing for different values of h/w were used, and four values of the fluid contact angle were chosen: two above the Concus–Finn limit ($\theta > 45°$) and two below the Concus–Finn limit. Above the Concus–Finn limit, it can be shown that fluid can either satisfy the conditions for SCF (Eq. **S6**) and cover the aperture or not satisfy the conditions for SCF and not cover the aperture (outlined in Fig. S5, *Upper*). Below the Concus–Finn limit, the fluid flows on either side of the aperture and the two filaments created have the possibility to merge and fill the aperture. For the geometry of the first channel, with a height of 50 μm, we find that SCF over the aperture never occurs regardless of the values of θ (Fig. S6, first column). In the second case, for a height of 100 μm, SCF does not occur for values of the contact angle above the Concus–Finn limit; however, below the Concus–Finn limit, the filaments can merge downstream of the aperture and cover it (Fig. S5, second column). In the third case, for a height of 150 μm, we find that SCF occurs above the Concus–Finn limit in good accordance with the prediction from Eq. **S6** and that below the Concus–Finn limit, the fluid is able to flow around and fill the aperture readily. These examples show the robustness of the final graph determined and described in Fig. 1*C*.

1. Duffy DC, McDonald JC, Schueller OJ, Whitesides GM (1998) Rapid Prototyping of Microfluidic Systems in Poly(dimethylsiloxane). *Anal Chem* 70(23):4974–4984.

2. Samandari E, et al. (2007) Human adrenal corticocarcinoma NCI-H295R cells produce more androgens than NCI-H295A cells and differ in 3beta-hydroxysteroid dehydrogenase type 2 and 17,20 lyase activities. *J Endocrinol* 195(3):459–472.

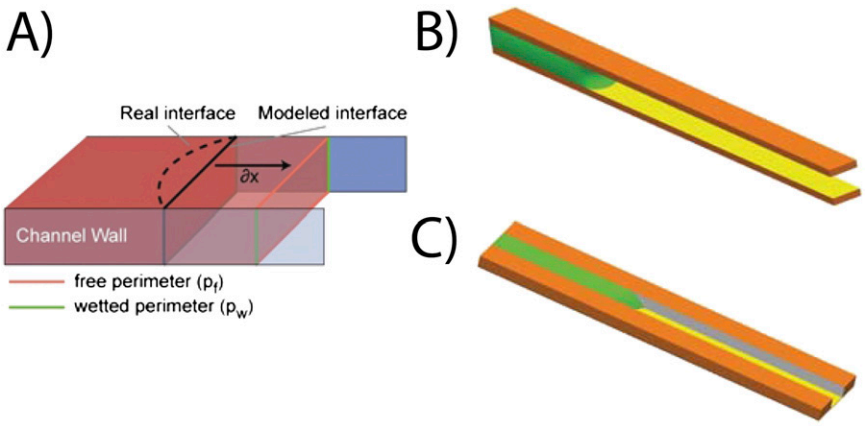

Fig. S1. (*A*) Advancement of the fluid front in an open microfluidic channel in which part of the cross-section represents solid walls and part represents open liquid–air interfaces. The interfaces are simplified to a straight line. Surface Evolver calculation for parallel rails (*B*) and a groove with a U-shaped cross-section (*C*). Note that Surface Evolver does not allow for dynamic computation of the flow; however, because it searches for the equilibrium position and morphology of the liquid interface, a Surface Evolver calculation predicts if the liquid is at rest or if the liquid surface changes toward another equilibrium position.

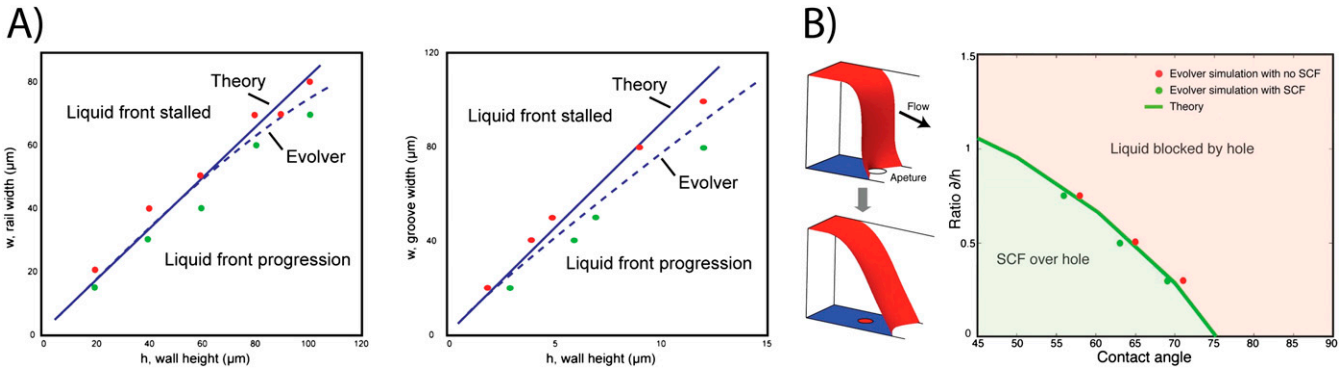

Fig. S2. (*A*) Comparison between the theoretical formulas and Surface Evolver numerical simulation results for parallel rails and a U-groove. The green dots signify that the liquid front progresses according to Surface Evolver, and the red dots signify that the front is stalled. The dotted blue line is the best-fit first-order polynomial function separating the green and red dots. The continuous line is the theoretical limit ($\theta = 35°$). (*B*) Comparison of the theoretical limit for SCF over an aperture for a range of different apertures and numerical simulations given by Surface Evolver software.

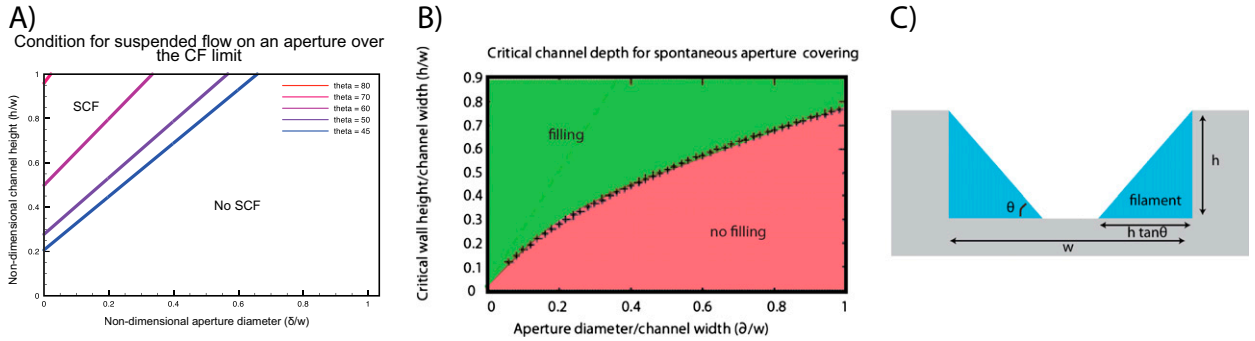

Fig. S3. (*A*) Parameter space plot of the conditions for SCF over an aperture in a U-shaped channel. For a given fluid of contact angle θ, SCF will occur for any geometry above the corresponding line. This supposes the simplification that the fluid flows as a bolus over the aperture and does not take into consideration the possibility for the fluid to flow around the aperture in two filaments, merge, and cover the aperture subsequently. (*B*) Surface evolver simulations show the filling for below the Concus–Finn Limit ($\theta < 45$), when the fluid acts to fill the wedges in the channel (*C*).

Geometry	Conditions for SCF	View
Parallel rail	$\frac{w}{h} < \cos(\theta)$	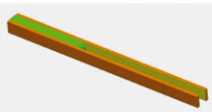
Parallel U-shaped groove	$\frac{w}{2h + w} < \cos(\theta)$	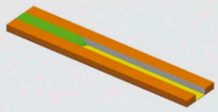
Diverging rail	$\frac{w_{end}}{h} < \cos(\theta)$	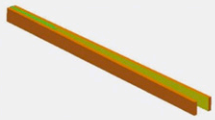
Converging rail	$\frac{w_{start}}{h} < \cos(\theta)$	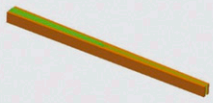
Diverging U-shaped groove	$\frac{w_{end}}{2h + w} < \cos(\theta)$	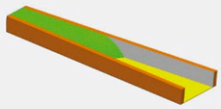
Converging U-shaped groove	$\frac{w_{start}}{2h + w} < \cos(\theta)$	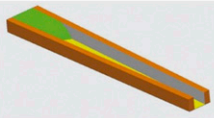
U-shaped groove with pinholes	$\begin{cases} \frac{w}{2h + w} < \cos(\theta) \\ \frac{h}{\delta} > 2.5 \end{cases}$	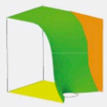

Fig. S4. Different spontaneous flows for different geometry channels, with (1) type of channel, (2) an equation describing the conditions for flow, and (3) a Surface Evolver schematic.

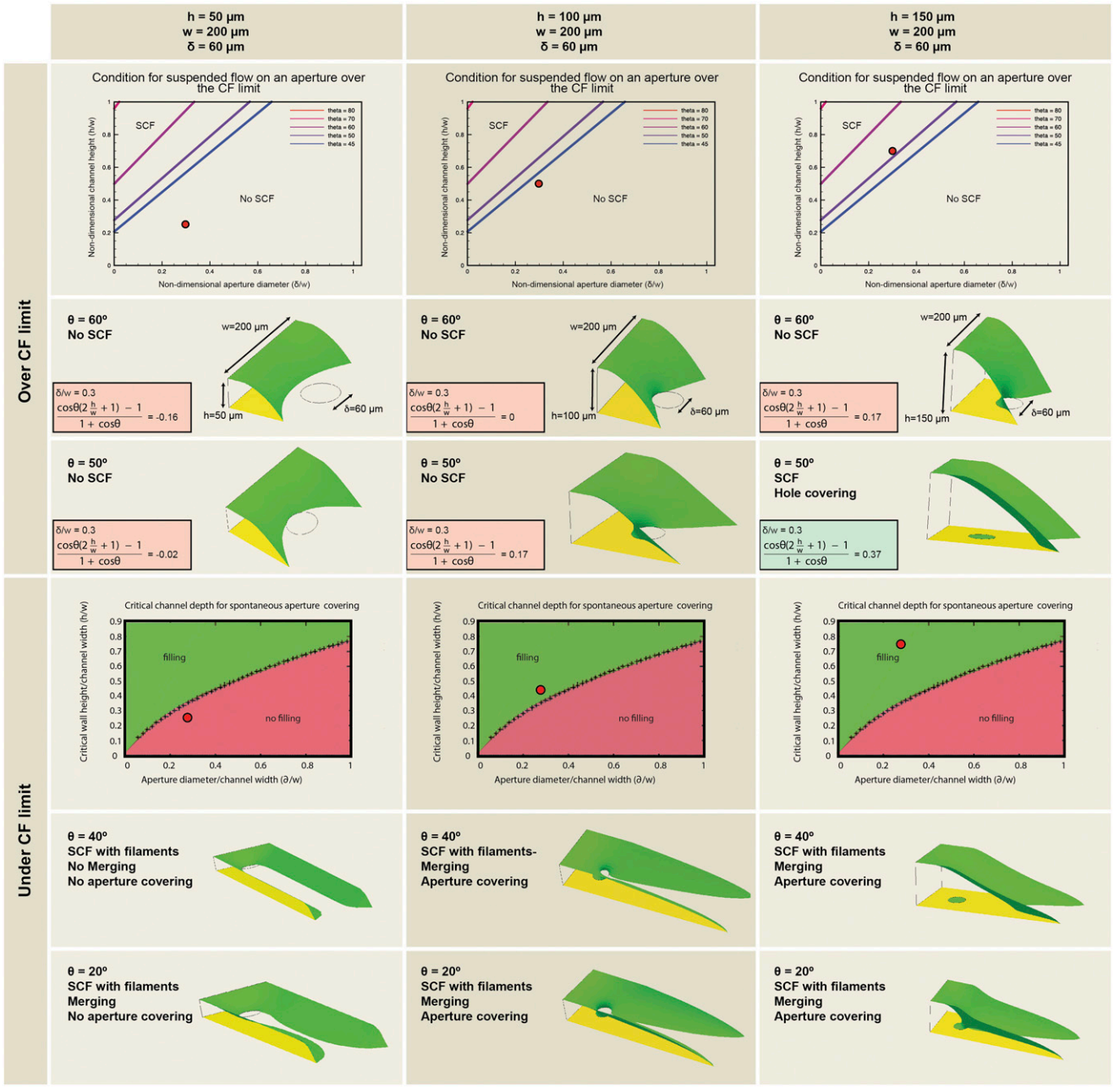

Fig. S5. Summary of aspect ratios for filling an aperture in a U-shaped channel.

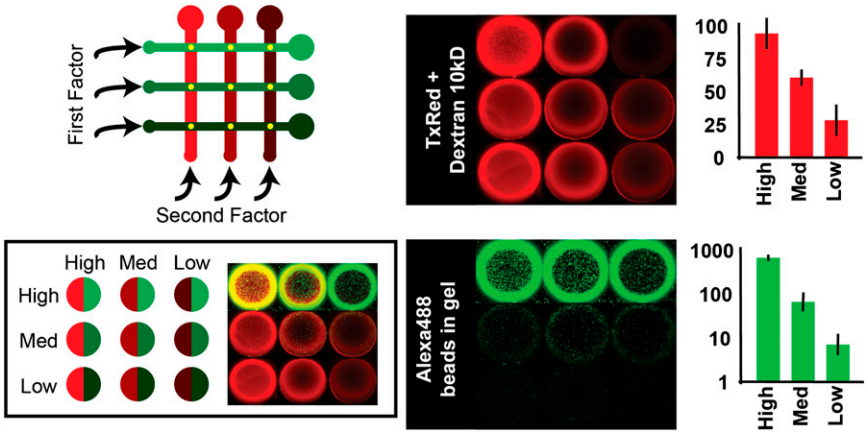

Fig. S6. Combinatorial assay demonstrates the addition of Texas Red dextran on one axis and FITC-bound silica beads on the other. Error bars represent SD of the mean (n = 3).

Table S1. HPLC binary gradient pump program for hormone analysis

Time, min	Channel B, %	Flow rate, mL/min
0	3	0.25
2	3	0.25
2.1	50	0.25
5	50	0.25
20	67	0.25
23	100	0.25
30	100	0.25
30.1	3	0.25
40	3	0.25

Channel A is 0.1% formic acid (Sigma–Aldrich), and channel B is methanol (Honeywell B&J).

Table S2. MS/MS parameters for multiple reaction monitoring analysis

Analyte	Q1, *m/z*	Q2, *m/z*	Dwell time, ms	DP, V	CE, V	CXP, V
Testosterone-1	289	97	20	126	29	14
Testosterone-2	289	109	20	126	33	16
Cortisol-1	363	77	20	171	103	32
Cortisol-2	363	91	20	171	83	12
Cortisol-3	363	121	20	171	31	14
Cortisone-1	361	163	20	111	33	26
Cortisone-2	361	77	20	111	111	12
Cortisone-3	361	91	20	111	89	14
11-DOC-1	347	97	20	186	31	18
11-DOC-2	347	109	20	186	43	14
Testosterone d5	294	100	20	71	33	6
Cortisol d4	367	121	20	36	31	20

One quantitative multiple reaction monitoring transition and at least one confirmatory multiple reaction monitoring transition were monitored for each analyte. CE, collision energy; CXP, collision cell exit potential; DOC, 11-deoxycorisol; DP, declustering potential; Q, quadrupole.